Ultrasonic meters in wet gas applications

Dennis van Putten, Henk Riezebos, René Bahlmann (DNV GL)

Jan Peters, Rick de Leeuw (Shell)

Joe Shen (Chevron)

DNV GL Oil & Gas
Energieweg 17, 9743 AN Groningen
dennis.vanputten@dnvgl.com

1 INTRODUCTION

Oil and gas operators today are facing a number of significant measurement challenges in their efforts to optimize production and generate more from their reservoirs, particularly in wet gas fields. Traditional flow measurement technologies in wet gas fields for well reservoir management (WRM) purposes are Venturi meters or orifice plate meters that involve differential pressure (dp) measurements. The advantage of these technologies is that the flow data can be generated under almost any wet gas process condition and that correction algorithms are available , refs [7] and [8]. There are some disadvantages in terms of limited rangeability, cost and pressure drop.

Many oil and gas operators are aware of the disadvantages and are investigating other options. In the past decade ultrasonic technologies, both inline as well as clamp-on, are being successfully applied in dry gas applications. The main advantages of the ultrasonic technology are the large rangeability (high turn-down ratio), (nearly) undisturbed flow patterns with absence of pressure drop, no obstructions or moving parts and powerful diagnostic features. Last decade also the clamp-on ultrasonic technology has made significant steps ahead in gas measurement applications.

Ultrasonic inline and clamp-on technologies have been applied in wet gas circumstances. Although promising first results are available, most ultrasonic technologies applied under wet gas conditions are currently mostly "trial and error" based and mainly focus on the performance in field applications. A systematic approach towards a correction for liquid fractions has been lacking so far.

Typical sales allocation industry requirements express the need to have allocated gas volumes determined with a maximum uncertainty of 2%. In practice it can be proven that the operational uncertainties of the wet gas flow meters are in the range of 2%-5% this can be considered as industry acceptable. However, a serious issue is to determine possible biases due to wet gas circumstances. Due to the liquid introduction the flow meters tend to over-read in terms of gas flow which can reach values of 20-30%. To systematically explore the application of ultrasonic flow meters in wet gas sales allocation applications, DNV GL has executed a Joint Industry Project (JIP) with E&P companies and ultrasonic manufacturers. The E&P companies that joined the project were NAM, Shell and Chevron. Both inline ultrasonic manufacturers: Daniel, Elster-Instromet, Krohne and Sick; and clamp-on ultrasonic manufacturers: Expro, Flexim and Siemens participated in this JIP.

A main goal of this JIP was to develop a correction algorithm to account for the expected over-reading of the ultrasonic meters due to the introduction of liquid. To develop the algorithm for the ultrasonic meters, a good understanding of the multiphase flow physics is needed to predict the behaviour of the liquid. The fundamental study on multiphase flow has led to a physical model for the liquid hold-up

and supported the development of the test setup and the test matrix. Test data of the participating ultrasonic meters has been generated during an extensive test campaign and was used to determine the parameters in the over-reading model. This paper will present the results of the ultrasonic meters tests and the obtained generic correction algorithm.

2 MULTIPHASE FLOW FUNDAMENTALS FOR WET GAS

The analysis of the multiphase flow equations is used to find analytic solutions of the liquid hold-up within certain limits, e.g. in stratified flow. Moreover, the analysis will demonstrate which parameters are important, from a fluid dynamical point of view, and therefore determine the setup of the test matrix. It will be shown that the number of independent parameters to be evaluated during the performance test can be reduced by means of a dimensional analysis.

The analysis of the multiphase flow equations is elaborated in Appendix A for a general two-phase flow. This analysis includes all encountered flow regimes of two-phase flow, where it is assumed that the liquid phase is well mixed and behaves as an emulsion, see Appendix B for the mixture rules. The next section considers the limiting case of the general derivation of Appendix A for wet gas.

2.1 Application to steady two phase gas-continuous flow

In the wet gas JIP tests the multiphase flow can be considered as gas-continuous and stationary. No significant pressure gradients are expected due to the full bore configuration of the ultrasonic meters. This information will allow for further reduction of the dimensionless numbers due to the absence of Sl_j and Eu_j, see Appendix A. In the case of wet gas, the gas and liquid flow equations are scaled by the same parameter, i.e. the $\rho_g u_{sg}^2 / D$. In the remainder of the derivation of the dimensionless equations the bar on the dimensionless variables will be omitted for clarity.

Applying dimensional analysis and this scaling results in the gas and liquid equation in dimensionless form

$$\nabla \cdot \left(\rho_g \boldsymbol{u}_g \boldsymbol{u}_g \right) = \frac{1}{\mathrm{Re}_g} \nabla \cdot \tau_g + \frac{1}{\hat{\mathrm{Fr}}_g^2} \rho_g \boldsymbol{g} \,, \tag{1}$$

$$\mathrm{X}_{\mathrm{LM}}^2 \nabla \cdot \left(\rho_l \boldsymbol{u}_l \boldsymbol{u}_l \right) = \frac{\mathrm{X}_{\mathrm{LM}}^2}{\mathrm{Re}_l} \nabla \cdot \tau_l + \frac{1}{\hat{\mathrm{Fr}}_g^2 \mathrm{DR}} \rho_l \boldsymbol{g} \,. \tag{2}$$

Also the jump condition can be written in dimensionless form by scaling with $\rho_g u_{sg}^2$ resulting in

$$\left(\frac{\mathrm{X}_{\mathrm{LM}}^2}{\mathrm{Re}_l} \tau_l - \frac{1}{\mathrm{Re}_g} \tau_g \right) \cdot \boldsymbol{n}_g = \frac{1}{\mathrm{We}_{\mathrm{g}}} \gamma \kappa \boldsymbol{n}_g \,, \tag{3}$$

where the Reynolds numbers, $\mathrm{Re}_{g/l}$, and the Froude number of the gas, $\hat{\mathrm{Fr}}_g$, were already found for the general two-phase equation in Appendix A. In equations **(2)** and **(3)**, additional dimensionless groups are identified for wet gas

$$\mathrm{X_{LM}} \equiv \sqrt{\frac{\rho_l}{\rho_g}}\frac{u_{sl}}{u_{sg}}, \tag{4}$$

$$\mathrm{DR} \equiv \frac{\rho_g}{\rho_l}, \tag{5}$$

$$\mathrm{We}_g \equiv \frac{\rho_g u_{sg}^2 D}{\gamma}, \tag{6}$$

which are termed the Lockhart-Martinelli parameter, the density ratio and the gas Weber number, respectively. It is noted that often the densimetric Froude number is used which is defined as

$$\mathrm{Fr}_g = \hat{\mathrm{Fr}}_g \sqrt{\frac{\mathrm{DR}}{1-\mathrm{DR}}}. \tag{7}$$

The total set of dimensionless numbers is

$$\mathrm{Re}_g,\ \mathrm{Re}_l,\ \mathrm{Fr}_g,\ \mathrm{X_{LM}},\ \mathrm{We}_g,\ \mathrm{DR}. \tag{8}$$

The scaling of the Froude number with the density ratio does not lead to density ratio independence, which is also a fundamental requirement of the Buckingham PI theorem.

3 TEST SETUP

The test facility used in this JIP is the MultiPhase Flow Laboratory of DNV GL in Groningen. A general description of the facility including an explanation of the flow rate reconstruction and uncertainty model can be found in ref [14]. The facility performs well for wet gas flow conditions and the uncertainties of the reference gas and liquid flow rates are well within 1%.

The study is limited to the wet gas regime, i.e. Gas Volume Fraction $\mathrm{GVF} > 95\%$ and $\mathrm{X_{LM}} < 0.3$. The tests in the JIP are performed at pressures between 12 and 32 bara in the temperature range between 15 and 35°C. The fluids used are natural gas, Exxsol D120 (API 40, 4.8cSt) and salt water with a salinity of 4%wt. In Figure 3-1 an example of a two phase flow regime map is depicted. For wet gas testing the flow regimes that are typically encountered are stratified (wavy) flow and dispersed flow.

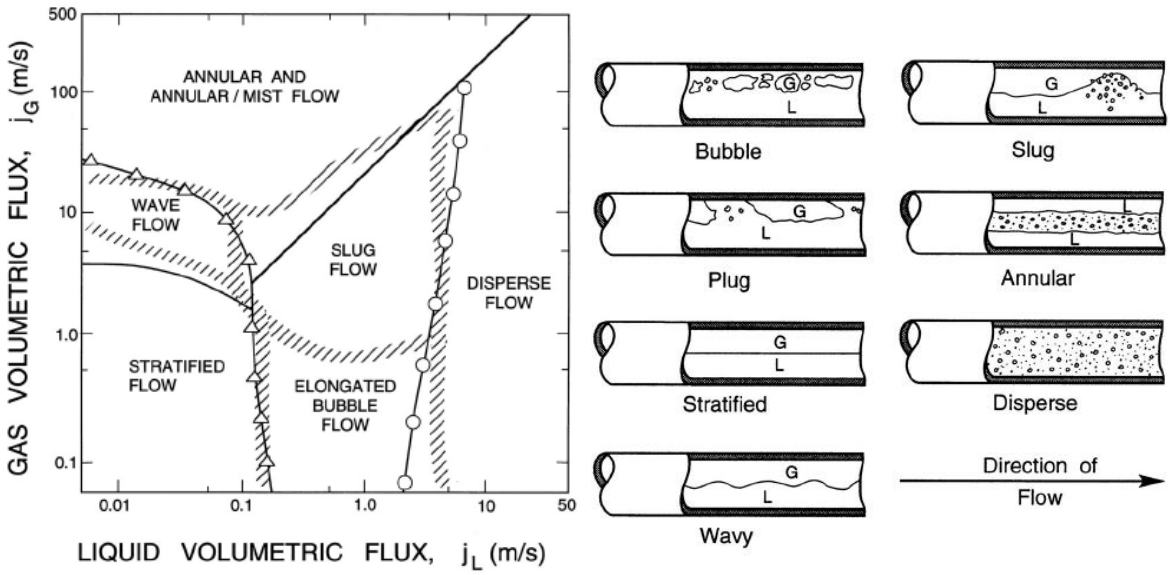

Figure 3-1 : Flow regime map for atmospheric air/water mixtures in horizontal configuration as a function of the phase volumetric flux (left) and corresponding flow patterns (right), figures from ref [2].

3.1 Test section design

All ultrasonic meters were installed in a single 6" test line in horizontal orientation, see Figure 3-2. To establish a level playing field it was mandatory to prove equal conditions for each flow meter. This was realized by taking sufficient upstream length from distorting elements, i.e. pipe elbows and temperature sensors, to provide fully developed multiphase flow and the same flow regime to each meter. This was validated by installing two optically accessible pipe sections upstream and downstream of the test section. The observed flow patterns with the optical pipe sections we used to validate the theoretical hold-up model. Possible risk of interference of ultrasonic signals between different flow meters was mitigated by installing the ultrasonic meters in order of alternating frequencies and taking sufficient distance between them.

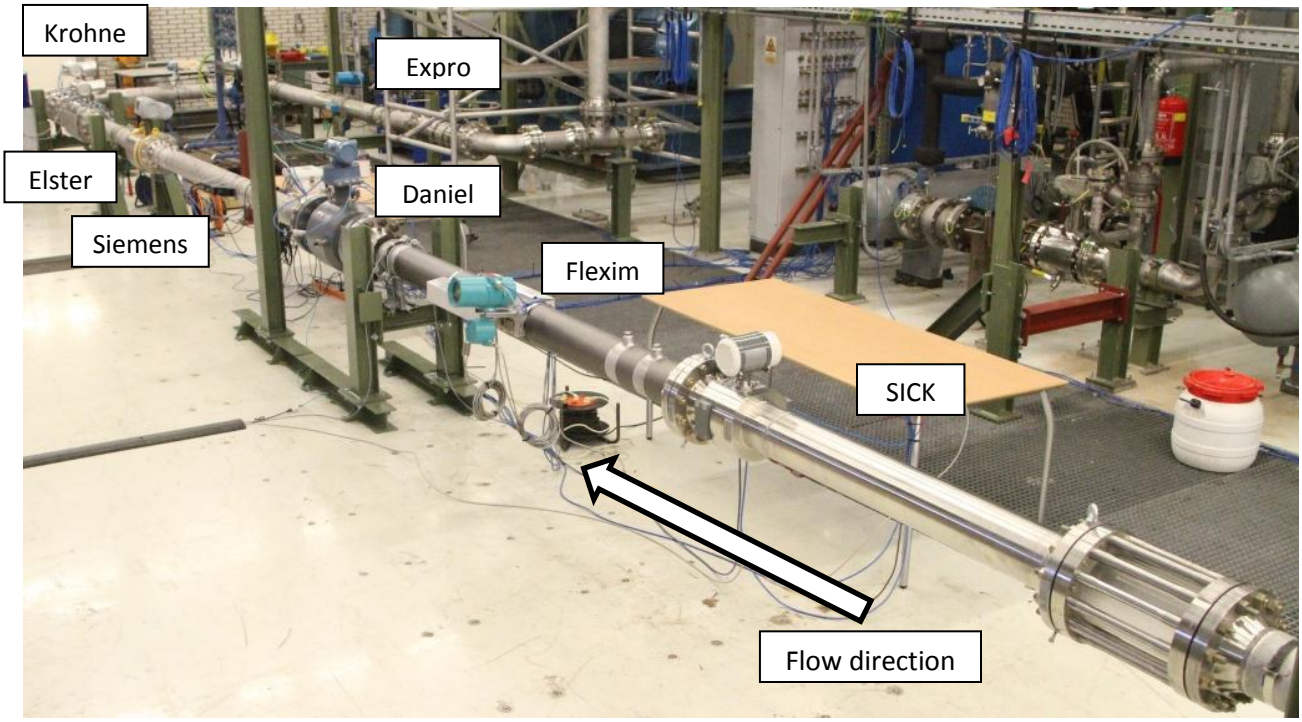

Figure 3-2 : Overview of JIP test setup at DNV GL test facility

3.2 Test matrix

The conventional methodology to define a test matrix is to specify dimension-full quantities like pressure, temperature and phase flow rates. Since the characteristic behaviour of a multiphase flow is not directly related to these quantities, a different approach is applied. In the previous section, it was explained how the multiphase flow equations can be written in dimensionless form and which dimensionless parameters determine the topology of the multiphase flow. For a gas dominated flow the expected dominant dimensionless quantities are:

$$\mathrm{Re}_g,\ \mathrm{Re}_l,\ \mathrm{Fr}_g,\ \mathrm{X}_{\mathrm{LM}},\ \mathrm{We}_g,\ \mathrm{DR}. \tag{9}$$

The core of the test matrix is constructed in terms of Fr_g, X_{LM} and DR with values that span the operational envelop of the test facility. The applied values for the test matrix are:

$$\begin{aligned} \mathrm{Fr}_g &= [0.7\ \ 1.2\ \ 1.7\ \ 2.2] \\ \mathrm{X}_{\mathrm{LM}} &= [0.01\ \ 0.02\ \ 0.04\ \ 0.08\ \ 0.15\ \ 0.3] \\ \mathrm{DR} &= [0.01\ \ 0.013\ \ 0.016\ \ 0.02\ \ 0.026\ \ 0.032] \end{aligned} \tag{10}$$

The Fr_g variation is chosen to span both the dispersed and stratified regime. The X_{LM} variation is chosen to cover the wet gas envelop and focus is laid on the low liquid content test points. The Fr_g and X_{LM} test points form the basis for the test matrix and the DR is chosen in such a way that the gas-oil density ratio at a certain pressure corresponds to the gas-water density ratio at a pressure one increment higher. Therefore, at a certain test point the difference between the properties of the oil

and water can be directed to the viscosity effect, i.e. Re_l, or the surface tension effect, i.e. We_g. A distinction between these two dimensionless numbers can be established by changing the temperature of the gas and oil flow. The viscosity of the oil is a strong function of temperature, whereas the surface tension varies only slightly. Also mixtures of oil and water are executed leading to high values of the viscosity near the oil-water inversion point. In total approximately 200 test points were run.

Two output signals were required from the flow meters: Actual volumetric flow rate and speed of sound. A stable test point with a duration of 10 minutes was logged, from which averages were taken for the correction algorithm analysis. During the test, the diagnostics of the ultrasonic meter were logged and based on this data the manufacturer provided a valid or invalid tag to each test point.

4 TEST RESULTS

Before commencing with the wet gas test matrix, a dry gas baseline test was performed to eliminate systematic deviations at single phase conditions. In the wet gas data only the valid test points will be presented in this paper and this data will be used for the development of the correction algorithm.

The over-reading is based on volumetric flow rates and is defined as:

$$\mathrm{OR} \equiv \frac{Q_g^{MUT}}{Q_g^{ref}}, \tag{11}$$

where Q_g^{MUT} is the measured gas volumetric flow rate by the ultrasonic meter and Q_g^{ref} is the actual gas volumetric flow rate given by the reference system of the test facility, both at line conditions. In Figure 4-1 the over-reading of all ultrasonic meters is plotted as a function of Fr_g and X_{LM}. In Figure 4-2 the projection of the results as a function of Fr_g and X_{LM} is plotted separately. The global behaviour of the ultrasonic meters is indicated by the green lines. Note that due to the projection the dependence in the other dimension might be misinterpreted as scatter. Also these results are for all liquid mixtures and all DR.

In Figure 4-2 a strong over-reading dependence is observed in terms of X_{LM}, with a maximum of 25-30%. For low Fr_g numbers, i.e. stratified flow, the over-reading becomes independent on Fr_g. Increasing the Fr_g number leads to atomization of the liquid which results in a lower liquid hold-up and consequently in a lower over-reading.

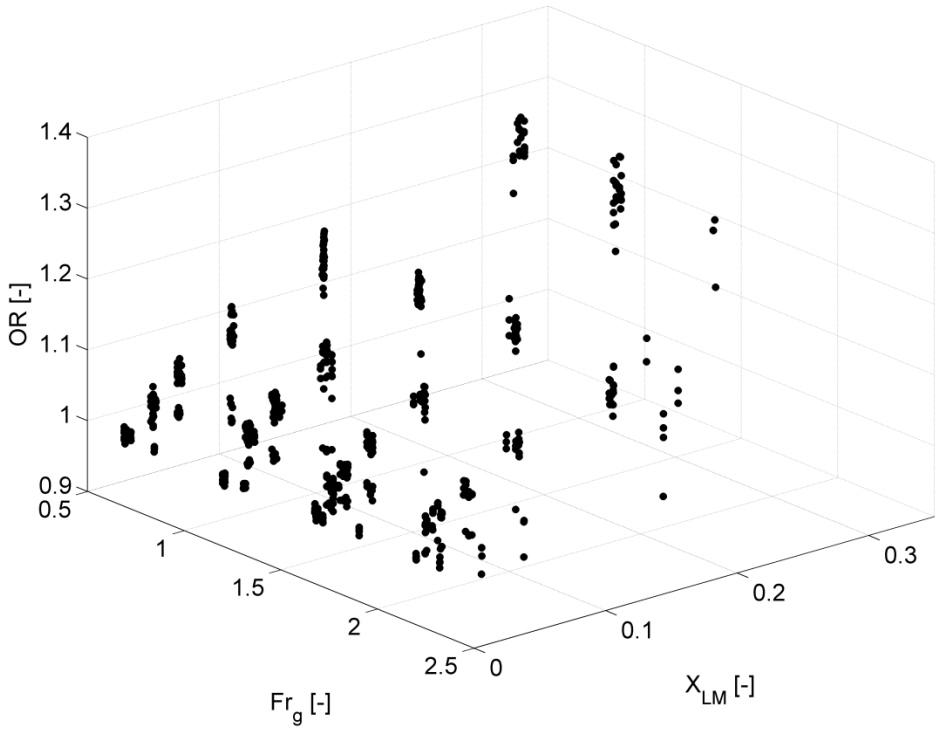

Figure 4-1 : Over-reading of all ultrasonic meters as a function of Fr_g and X_{LM}.

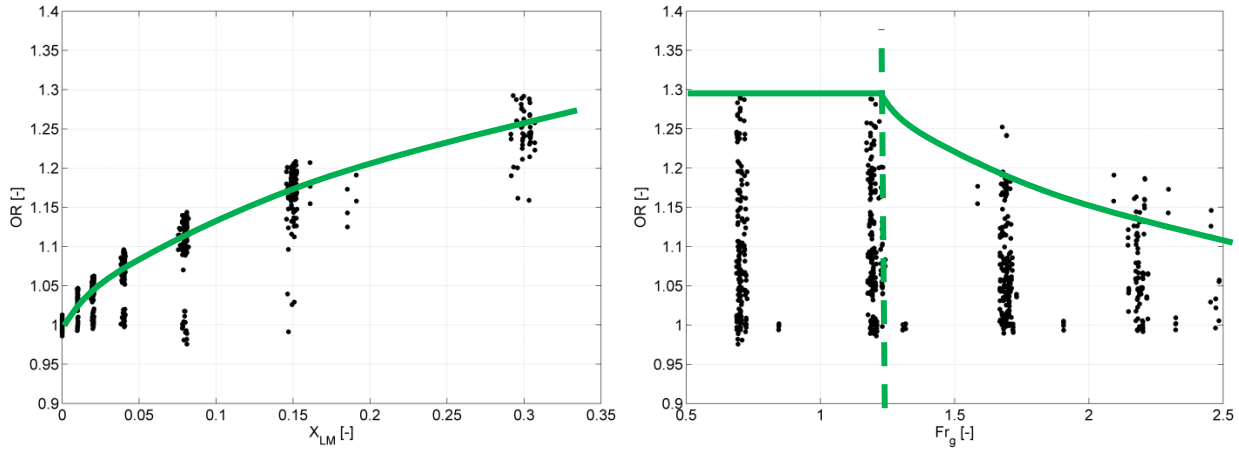

Figure 4-2 : Projection of over-reading of ultrasonic meters as a function X_{LM} (left) and Fr_g (right). The green solid lines indicate the global behaviour and the green dashed line indicates the transition point.

5 DEVELOPMENT OF CORRECTION ALGORITHM

The over-reading of the ultrasonic meters is assumed to be directly proportional to the liquid hold-up, or in terms of the gas void fraction, α_g ,

$$\mathrm{OR} \equiv \frac{Q_g^{MUT}}{Q_g^{ref}} = \frac{1}{\alpha_g}. \tag{12}$$

Since an ultrasonic flow meter measures the velocity, the reconstruction of the volumetric flow rate is not evident in a wet gas environment. For the development of the correction algorithm, we assume that the resulting gas velocity profile is flat and that the ultrasonic meter does not correct internally for the presence of the liquid phase. Also, it is assumed that the velocity measurement itself is not influenced by the multiphase flow, i.e. the liquid will cause the signal to be attenuated but it will not have an influence on the speed of sound and therefore produce a valid velocity measurement. The latter can be proven to be true for sufficiently high frequencies, see refs [9] and [16].

5.1 General construction of the correction algorithm

The procedure of constructing the correction algorithm is based on the principle of separation of variables. Application of this method results in a set of functions that depend solely on a single dimensionless number. For the gas void fraction one can write

$$\alpha_g = \chi(\mathrm{X_{LM}})\phi(\mathrm{Fr}_g)\omega(\mathrm{We}_g)\Delta(\mathrm{DR})\xi(\mathrm{Re}_g)\eta(\mathrm{Re}_l)\,. \tag{13}$$

The function expression in **(13)** should obey different physical limits. The first set of conditions the function should satisfy are based on Fr_g and $\mathrm{X_{LM}}$, since these parameters are expected to be of main influence

$$\begin{aligned} &\lim_{X_{LM}\to 0} \alpha_g = 1 \\ &\lim_{X_{LM}\to \infty} \alpha_g = 0 \\ &\lim_{Fr_g\to 0} \alpha_g = \mathrm{stratified\,flow} \\ &\lim_{Fr_g\to \infty} \alpha_g \approx \mathrm{GVF} \end{aligned} \tag{14}$$

The limits of $\mathrm{X_{LM}}$ and stratified limit of Fr_g are evident, whereas the limit of Fr_g to infinity needs further explanation. For large Fr_g the liquid is assumed to be dispersed and the velocity of the liquid approaches the gas phase velocity and therefore the gas void fraction will tend to the gas volume fraction. It should be noted that a liquid film will be present on the wall and this results in a lower velocity of the liquid phase.

5.1.1 Stratified flow

A model has been developed for the gas void fraction in the stratified regime and is based on the fundamental equations as described in section 2, see refs [12] and [18]. The model indicates that the correction algorithm in the stratified flow regime should depend mainly on X_{LM} with some minor dependence on the ratio of the Reynolds numbers and the density ratio. The model by Van Maanen presented in ref [11] provides a simplification of stratified flow equations and gives for the gas void fraction

$$\tilde{\chi}_m(\mathrm{X}_{\mathrm{LM}}) = \frac{1}{1+\mathrm{X}_{\mathrm{LM}}}. \qquad \textbf{(15)}$$

The model developed in this study requires the solution of a set of non-linear equations and depends also on the Reynolds number ratio and the density ratio. The function is simply expressed as

$$\chi_m(\mathrm{X}_{\mathrm{LM}}, \mathrm{Re}_l / \mathrm{Re}_g, \mathrm{DR}). \qquad \textbf{(16)}$$

It is clear that the Van Maanen expression satisfies the limits in equation **(14)**. The same can be proven for equation **(16)**. For illustration purposes both expressions are plotted in Figure 5-1.

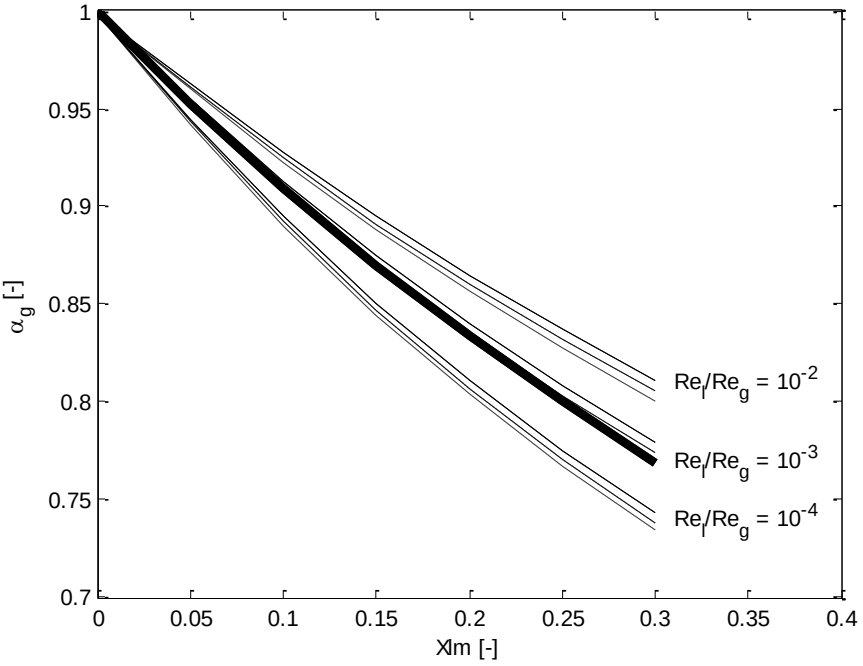

Figure 5-1 Gas void fraction from Van Maanen (equation (15)) : thick solid line, and from equation (16) for different DR: 0.015 (solid line), 0.025(dashed line) and 0.035 (dotted line) and different Re_l/Re_g.

Using the data from the JIP testing, it is observed that a systematic error remains in terms of X_{LM} after correction with the theoretical models in equations **(15)** and **(16)**, see Figure 5-2. The reason for this error can be found in the theoretical construction of both stratified flow models. The

expression by Van Maanen does not take into account viscous effects, while for low $\mathrm{X_{LM}}$ and thus low liquid hold-up the contact surface of the liquid is large compared to the bulk liquid flow. Viscous effects will increase the hold-up and therefore produce a larger over-reading. The expression developed by DNV GL does include viscous stresses, but require as input the hydraulic diameter of the liquid flow. This diameter is not well defined for low liquid hold-up. Increasing $\mathrm{X_{LM}}$ results in a better agreement with the experimental data.

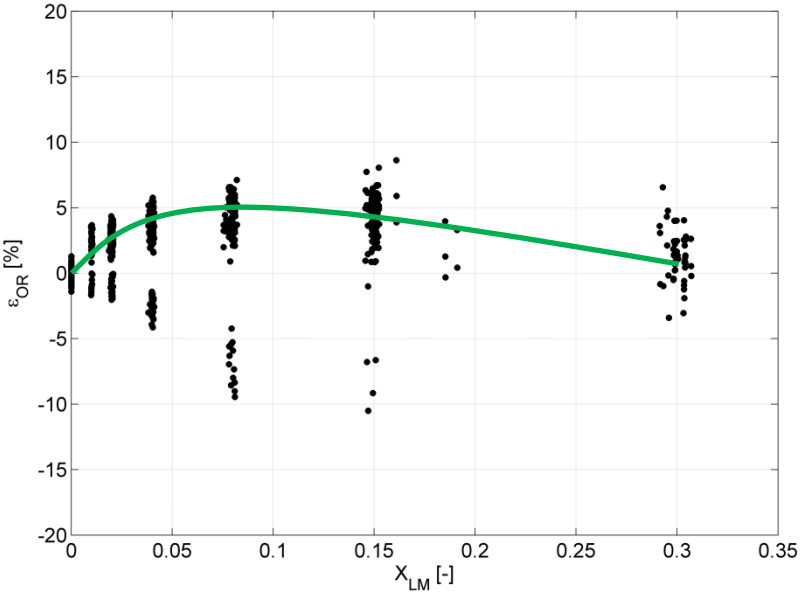

Figure 5-2 : Systematic error in OR after correction by χ_m for stratified flow (low Fr_g), green line indicates trend

An additional correction is required to improve the predictability of the model. A polynomial expression capable of correcting this function is given by

$$\begin{aligned} &\chi_a = -\mathrm{X}_{\mathrm{LM}}^{b_1} + b_2 \mathrm{X}_{\mathrm{LM}} \\ &0 < b_1 < 1 \\ &b_2 > 0 \end{aligned} \quad . \tag{17}$$

For both expressions (equations **(15)** and **(16)**) the parameters can be fitted to minimize the error, resulting in

$$\begin{aligned} \tilde{\chi}_a &= -\mathrm{X}_{\mathrm{LM}}^{0.76} + 1.44\mathrm{X}_{\mathrm{LM}} \\ \chi_a &= -\mathrm{X}_{\mathrm{LM}}^{0.75} + 1.35\mathrm{X}_{\mathrm{LM}} \end{aligned} \quad . \tag{18}$$

The final expressions for both χ -functions are constructed as

$$\chi = \chi_m + \chi_a \, . \tag{19}$$

5.1.2 Dispersed flow

The limit towards high Fr_g -numbers is covered in the $\phi(\mathrm{Fr}_g)$ function. For low values of Fr_g, the expression for stratified should remain unaltered and therefore

$$\phi(\mathrm{Fr}_g) = 1 \tag{20}$$

for values of Fr_g lower than a critical value, denoted by Fr_g^*. The transition of the stratified regime towards the disperse regime is covered by an exponential function since it is expected that the onset of the transition is relatively quick whereas the asymptotic behaviour of establishment of the dispersed flow regime will be slowly attained. The following expression is proposed

$$\phi(\mathrm{Fr}_g) = \begin{cases} 1 & \mathrm{Fr}_g < \mathrm{Fr}_g^* \\ (1-c_1)\exp[-c_2(\mathrm{Fr}_g - \mathrm{Fr}_g^*)] + c_1 & \mathrm{Fr}_g \geq \mathrm{Fr}_g^* \end{cases} \tag{21}$$

where the constant c_1 is determined by the limit

$$\lim_{Fr_g \to \infty} \alpha_g = \lim_{Fr_g \to \infty} \left[\chi(\mathrm{X_{LM}}) \phi(\mathrm{Fr}_g) \right] = \mathrm{GVF}, \tag{22}$$

and so

$$\lim_{Fr_g \to \infty} \phi(\mathrm{Fr}_g) = c_1 = \frac{\mathrm{GVF}}{\chi(\mathrm{X_{LM}})}. \tag{23}$$

The c_2 constant in equation **(21)** determines the rate at which the flow regimes transit from stratified to disperse. This parameter is fitted to the JIP data, resulting in: $c_2 = 0.4$. It is clear that due to the matching of the boundary conditions, ϕ also becomes a function of $\mathrm{X_{LM}}$ and DR.

5.1.3 Transition point

The critical Froude number, Fr_g^*, is determined by considering the important factors of the transition process between stratified and disperse. Typically, $\mathrm{Fr}_g^* = 1.2$ for gas-oil flows and $\mathrm{Fr}_g^* = 1.5$ for gas-water flows, see ref [7]. An obvious choice would be to linearly interpolate these values with the WLR. However, this is not a generic approach. It is known that interface instabilities cause the break-up of the interface into droplets. Two dominant dimensionless numbers play a role in this process: Re_g and We_g. The Re_g determines the shear force exerted on the interface by the gas stream, the We_g determines the forces exerted by the surface tension to keep the interface flat. One can again construct physical limits which the equation for the Fr_g^* should satisfy

$$\lim_{\mathrm{Re}_g \to \infty} \mathrm{Fr}_g^* = \infty \qquad (\text{inviscid gas} : \mu_g = 0)$$
$$\lim_{\mathrm{We}_g \to \infty} \mathrm{Fr}_g^* = 0 \qquad (\text{surface tension} : \gamma = 0)$$
$$\lim_{\mathrm{We}_g \to 0} \mathrm{Fr}_g^* = \infty \qquad (\text{surface tension} : \gamma = \infty) \tag{24}$$

Equations **(24)** indicate that an inviscid flow, $\mu_g = 0$, cannot exert a force on the interface and therefore the flow will remain stratified, i.e. $\mathrm{Fr}_g^* = \infty$. The same accounts for an infinite surface tension, γ, leading to $\mathrm{We}_g = 0$. When the surface tension tends to zero, i.e. $\mathrm{We}_g = \infty$, the interface will instantaneously break-up in small droplets. Combining both dimensionless numbers to the Ohnesorge number

$$\mathrm{Oh}_g \equiv \frac{\sqrt{\mathrm{We}_g}}{\mathrm{Re}_g} = \frac{\mu_g}{\sqrt{\rho_g \gamma D}} . \tag{25}$$

The Oh_g number is often used in jet break-up and atomization problems; see e.g. refs [1] and [15]. The limits defines in equations **(24)** convert to limits for the Oh_g number and a function that satisfies these limits is given by

$$\mathrm{Fr}_g^*\left(\mathrm{Oh}_g\right) = c_3 \mathrm{Oh}_g^{-c_4} . \tag{26}$$

By means of data fitting the coefficients are determined: $c_3 = 2.3 \cdot 10^{-5}$ and $c_4 = 1.1$. For other break-up processes it is known that c_4 is of the order of unity, see ref [1].

One could apply a simplification of equation **(26)** by using the fact that $\mathrm{Fr}_g^* = 1.2$ for gas-oil flows and $\mathrm{Fr}_g^* = 1.5$ for gas-water flows and using a WLR dependent interpolation

$$\mathrm{Fr}_g^* = 1.2 + 0.3\mathrm{WLR} . \tag{27}$$

5.2 Generic correction algorithm

The generic correction algorithm is now build-up from equations **(19)**, **(21)** and **(26)**

$$\alpha_g = \chi(\mathrm{X}_{\mathrm{LM}}, \mathrm{Re}_l / \mathrm{Re}_g, \mathrm{DR})\phi(\mathrm{Fr}_g, \mathrm{X}_{\mathrm{LM}}, \mathrm{DR}, \mathrm{Oh}_g) . \tag{28}$$

The generic correction algorithm involves all physical processes that were described in the previous sections. The algorithm is complex and requires the solution of a system of equations and detailed knowledge of the physical properties of the fluids.

Based on several simplifications proposed in this section one can construct an algebraic expression which is capable of correcting for the over-reading to a large extent while maintaining the main

physical background of equation **(28)**. For the dependence in terms of $\mathrm{X_{LM}}$, equation **(15)** combined with **(18)** is used. Then, using equation **(21)** with the simplification proposed in **(27)** leads to

$$\tilde{\alpha}_g = \begin{cases} \tilde{\chi}(\mathrm{X_{LM}}) & \mathrm{Fr}_g < \mathrm{Fr}_g^* \\ [\tilde{\chi}(\mathrm{X_{LM}}) - \mathrm{GVF}]\exp[-0.4(\mathrm{Fr}_g - \mathrm{Fr}_g^*)] + \mathrm{GVF} & \mathrm{Fr}_g \geq \mathrm{Fr}_g^* \end{cases} \quad \textbf{(29)}$$

where

$$\tilde{\chi}(\mathrm{X_{LM}}) = \frac{1}{1+\mathrm{X_{LM}}} - \mathrm{X_{LM}^{0.76}} + 1.44\mathrm{X_{LM}} \approx 1 - \mathrm{X_{LM}^{0.71}} + 0.73\mathrm{X_{LM}} \quad \textbf{(30)}$$

$$\mathrm{Fr}_g^* = 1.2 + 0.3\mathrm{WLR}$$

The latter part of the $\tilde{\chi}$-function is an approximation by means of a data fit to the original expression which was based on the physical description of the hold-up.

5.2.1 Application of the generic correction algorithm

Using the simplified correction algorithm instead of the generic correction algorithm based on the physical model results in relative modest differences. The corrected results using the generic model in equation **(28)** are depicted in Figure 5-3 and Figure 5-4. The error is defined as

$$\varepsilon_{\mathrm{OR}} = \mathrm{OR}\alpha_{\mathrm{g}} - 1. \quad \textbf{(31)}$$

The reconstruction of the data with the current correction algorithm results in a data set without additional systematic behaviour in other dimensions of the parameters space. The analysis included both the dimensional and the dimensionless parameters. Other observed variations are considered to be uncorrelated and can be considered as scatter. Also small systematic errors between different manufacturers are observed.

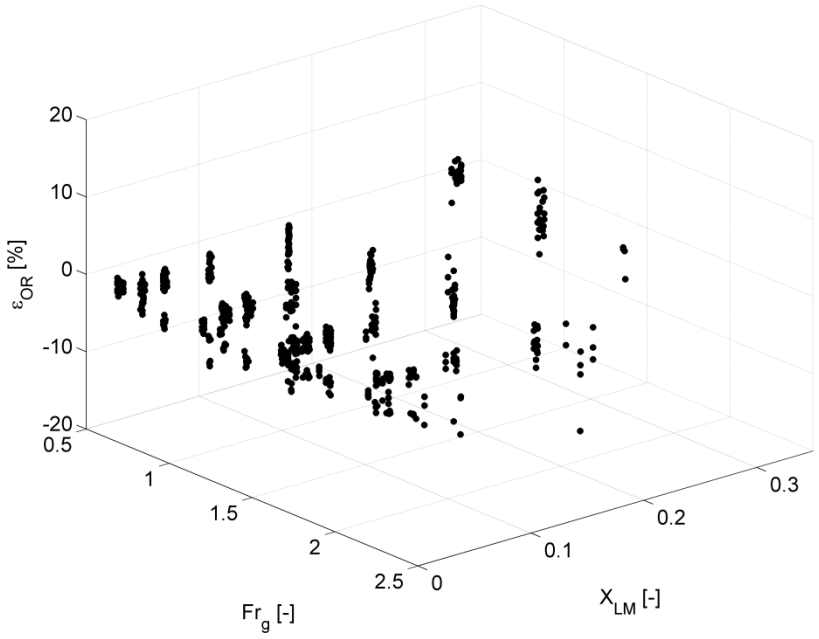

Figure 5-3 : Corrected over-reading of all ultrasonic meters as a function Fr_g and X_{LM}

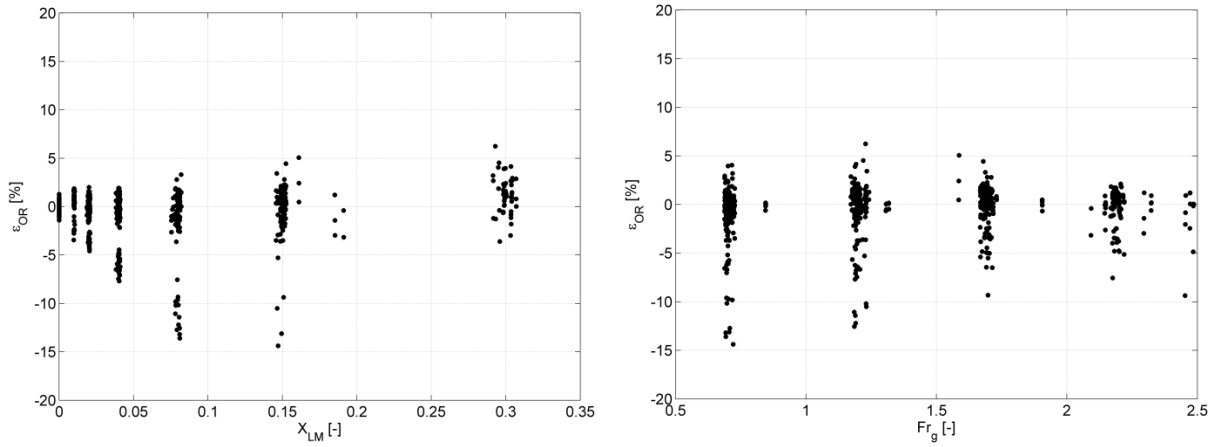

Figure 5-4 : Projection of corrected over-reading of the ultrasonic meters as a function X_{LM} (left) and Fr_g (right)

Most of the ultrasonic meters performed similarly as can be observed from Figure 5-4, which will be denoted by the core group of ultrasonic meters. Some meters demonstrate different behaviour, which can be assigned to differences in path configuration or the ability to already correct partly for the presence of liquid. Applying the over-reading correction to the core group of ultrasonic meters leads to low uncertainty on the gas volumetric flow rate. It is observed from Figure 5-3 and Figure 5-4 that the dependence on Fr_g and X_{LM} has been eliminated with exception of the small region near $\mathrm{X}_{\mathrm{LM}} = 0$.

The uncertainty of the corrected over-reading is determined on the basis of a 95% confidence interval. For the calculation only the valid test points are used, i.e. green labelled data. It is important to take into account these results together with the number of valid test points, since a conservative choice in approval of the test data may result in low uncertainty values and vice versa. For the core group of ultrasonic meters approximately 90% of all the data points were labelled green and the uncertainty is within 4%. Most of the red labelled data points are found at high Fr_g and high X_{LM}. It is obvious that the ultrasonic meters have problems at high X_{LM}, since this indicates high liquid volume fractions. The high Fr_g numbers can be explained by the transition to annular flow in which the ultrasonic signal is scattered and no valid data is obtained.

5.2.2 Extension of the correction algorithm

The applicability of the correction algorithm outside the operational envelop covered in the JIP test can be verified by using the data from the literature study. It should be noted that all the data has been supplied by the manufacturers (either via papers and conference proceedings or directly) so the data is not fully objective. Moreover, no validation of the test points has been performed in the same line as the traffic light system. The data of Cameron in ref [3], Flexim in ref [5], SICK in ref [10] and Daniel in ref [19] have been added to Figure 5-5. A surface plot is added to visualize the shape of the correction function. The corrected results are given in Figure 5-6.

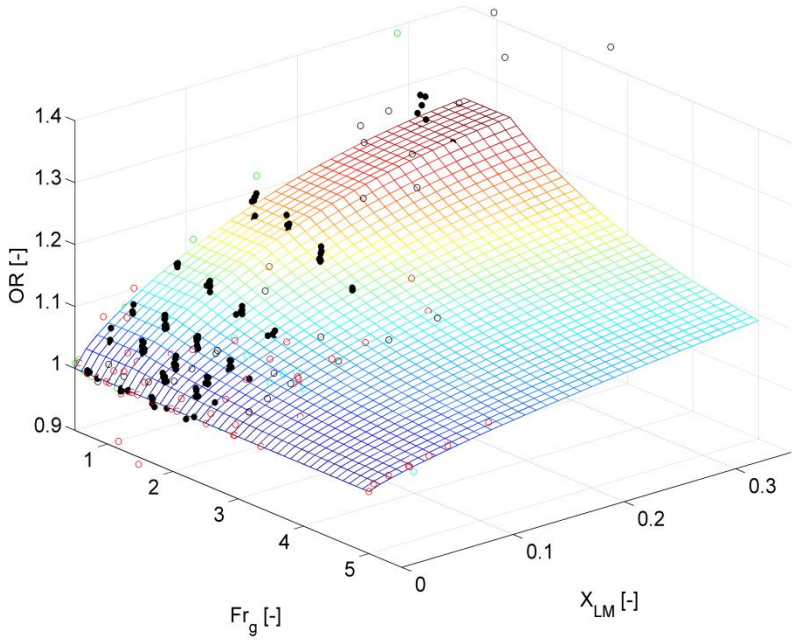

Figure 5-5 : Over-reading of ultrasonic meters as a function Fr_g and X_{LM} (black dots) including literature data (circles); green from ref [3], red from ref [5], black from ref [10] and blue from ref [19]. Surface plot is to indicate the shape of the correction algorithm.

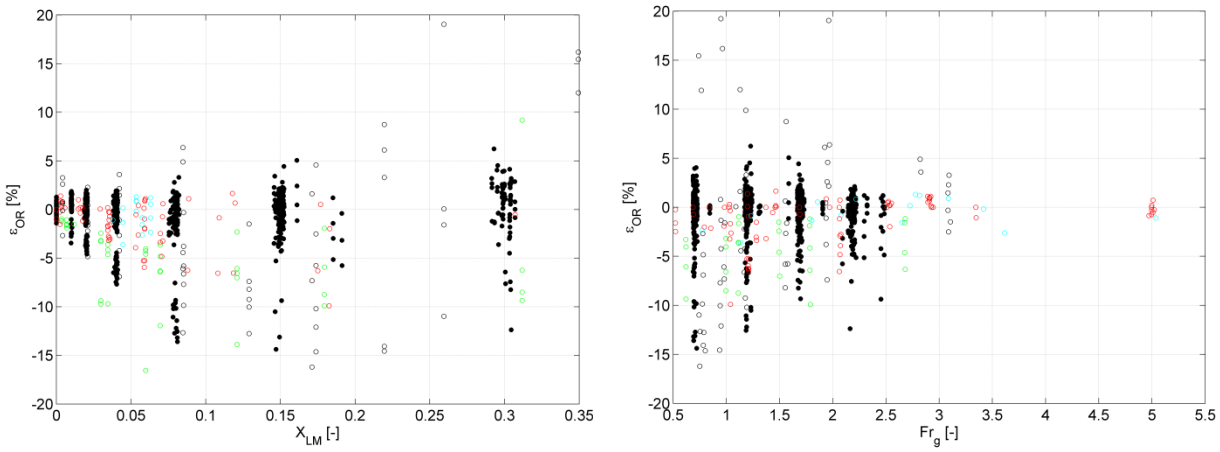

Figure 5-6 : Projection of corrected over-reading of ultrasonic meters as a function X_{LM} (left) and Fr_g (right) including literature data (circles); green from ref [3], red from ref [5], black from ref [10] and blue from ref [19]

As discussed before, it is difficult to use literature data when all information about the performed test is not available. Some of the literature data demonstrate large scatter, especially at low Fr_g -numbers which is surprising since at those conditions stratified flow is expected. The interesting part of Figure 5-6 is the high Fr_g -number limit in which the correction algorithm seems to predict the over-reading behaviour very well.

6 CONCLUSIONS

DNV GL has successfully executed the JIP on ultrasonic meters in wet gas applications. The aim of the project was to gain knowledge to support the wider use of ultrasonic meters in wet gas and to develop a correction algorithm to account for the expected over-reading of the ultrasonic meters due to the introduction of liquid.

To achieve these goals a test program was executed. In general, the ultrasonic meters are capable of handling the wet gas flow regimes and the resulting over-reading due to the additional liquid phase has a systematic character. It has been observed that the liquid hold-up in the test section reaches levels of approximately 30% of the cross sectional area leading to similar values for the over-reading of the gas flow rate. Due to the cusp shaped interface, the liquid layer near the wall can reach levels near the centreline of the pipe. Flow meters with ultrasonic paths under the centreline will experience problems with their signal when traversing the wet gas envelope. Therefore, the consistent over-reading results are obtained when considering velocity measurements in the domain above and including the centreline of the pipe. Results show that a generic correction algorithm is feasible as long as the ultrasonic path configurations are sufficiently similar.

A core group of ultrasonic meters has been identified which demonstrated corresponding over-reading data. These meters perform well in term of the number of valid test points, typically above 90%. Also, these meters showed good repeatability in wet gas and are capable of recovering the correct dry gas flow rate after a wet gas test point.

To develop the correction algorithm a test matrix was constructed in terms of dimensionless numbers. The analysis of the fundamental equations of multiphase flow indicated which dimensionless numbers are dominant and formed the basis for the test matrix.

The generic correction algorithm is based on a physical model of the two-phase flow and depends on the dimensionless numbers. The over-reading of the core group of ultrasonic meters is systematic and after application of the generic correction algorithm the resulting uncertainty of the gas flow rate is below 4% for all of the conditions tested. Data from literature is used to verify the correction algorithm for different diameters and higher pressures and showed reasonably good results. The ultrasonic meters that do not belong to the core group of ultrasonic meters demonstrate different behaviour which can be assigned to different path configurations or the ability to already compensate partly for the presence of liquid.

7 REFERENCES

[1] E. Badens , O. Boutin, and G. Charbit, Laminar jet dispersion and jet atomization in pressurized carbon dioxide*, J. of Supercritical Fluids*, 36 81, (2005).

[2] C.E. Brennen, *Fundamentals of Multiphase Flow* (Cambridge University Press, New York, 2005).

[3] G. Brown. Wet Gas Testing of an 8-path Ultrasonic meter. *Wet Gas Flow Measurement Workshop* (2011).

[4] E. Buckingham, On physically similar systems; illustrations of the use of dimensional equations. *Phys. Rev.* 4:345–376 (1914).

[5] B. Funck. Report on Testing Carried Out at the CEESI Wet Gas Test Facility in Colorado. *Internal Report* (2010).

[6] M. Ishii, *Thermo-fluid dynamic theory of two-phase flow* (Springer Verlag, Berlin, 2011).

[7] ISO TR 12748, *Wet Gas Flow Measurement in Natural Gas Operations,* Technical report Draft (2014).

[8] ISO TR 11583, *Measurement of wet gas flow by means of pressure differential devices inserted in circular cross-section conduits,* Technical Report (2012).

[9] L.E. Kinsler, A.R. Frey, A.B. Coppens, and J.V. Sanders, *Fundamentals of Acoustics* (John Wiley & Sons, New York, 2000)

[10] J. Lansing, T. Dietz, and R. Steven. Wet Gas Test Comparison Results of Orifice Metering Relative to Gas Ultrasonic Metering *NSFMW 1.2* (2010).

[11] H. de Leeuw, R. Steven, and H. van Maanen, Venturi Meters and Wet Gas Flow, NSFMW (2011)

[12] R. Malekzadeh, *Severe Slugging in gas-liquid two-phase pipe flow,* PhD Thesis, TU Delft (2012).

[13] A. Prosperetti, and G. Trygvasson, *Computational Methods of Multiphase Flow* (Cambridge University Press, New York, 2007).

[14] D.S. van Putten, *Flow Rate Reconstruction and Uncertainty Model of the MultiPhase Flow Facility Groningen*, GCS-2013-2111C (2014).

[15] M.A. Rahman, *Scaling of Effervescent Atomization and Industrial Two-Phase Flow*. PhD Thesis, University of Alberta (2011).

[16] S. Temkin, and R.A. Dobbins, Attenuation and Dispersion of Sound by Particulate-Relaxation Processes, *J. Acoust. Soc. Am.* 40:317-324 (1966).

[17] Y. Wang, and M.A. Oberlack. Thermodynamic Model of Multiphase Immiscible Flows with Moving Interfaces and Contact Line, *unpublished*, 2011.

[18] S. Wongwises, W. Khankaew, and W. Vetchsupakhun. Prediction of Liquid Holdup in Horizontal Stratified Two-Phase Flow. *J. Sc. Tech*. 3:2 (1998).

[19] K.J. Zanker, and G. Brown. The Performance of a Multi-Path Ultrasonic Meter with Wet Gas. *NSFMW 6.2* (2000).

APPENDIX A FUNDAMENTAL MULTIPHASE FLOW EQUATIONS

The derivation of the fundamental equations of multiphase flow starts with the local instantaneous formulation. This formulation states that the single phase flow equations are valid in the pure phase sub-regions of the domain under consideration, with exception of the interface, see refs [6] and [13]. The evaluation of the balance equations across the interface results in the so-called jump conditions. A schematic drawing of a multiphase mixture is given in Figure A-1.

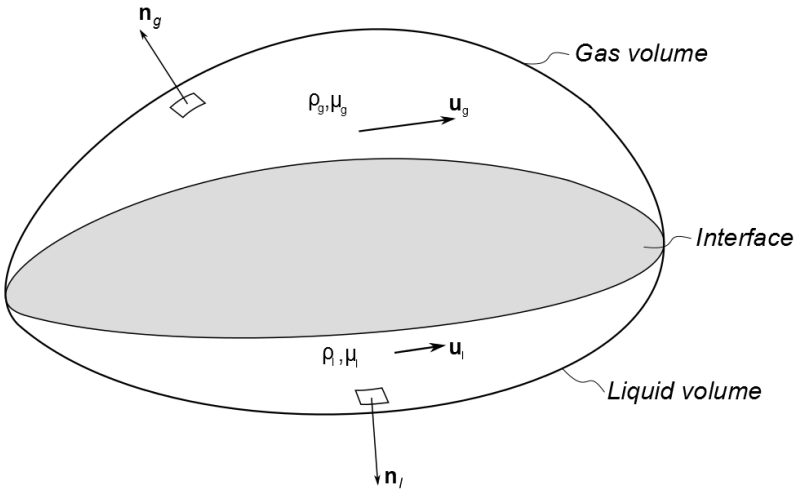

Figure A-1 Control volume of a two phase flow with upper gas phase sub-region and lower liquid phase sub-region separated by the gas-liquid interface.

In this study the multiphase flow mixture of gas, oil and water will be considered as a two-phase gas-liquid mixture, assuming that the water-oil mixture is an emulsion, which is valid for relatively high volumetric flow rates of the liquid phases. The liquid properties are determined by appropriate mixing rules, see Appendix B.

A general expression for the phase *j* (gas or liquid) is given by

$$\frac{\partial \rho_j f_j}{\partial t} + \nabla \cdot \left(\rho_j f_j \boldsymbol{u}_j \right) = \nabla \cdot \varphi_j + \rho_j \theta_j, \qquad j = g, l \tag{32}$$

with jump condition at the interface

$$-\sum_{j=g,l} \varphi_j \cdot \boldsymbol{n}_j = \gamma \kappa \boldsymbol{n}_g \tag{33}$$

where ρ_j, $\boldsymbol{u}_j$ and $\boldsymbol{n}_j$ are the mass density, velocity and unit outward normal of phase *j*, respectively. The values of f_j, φ_j and θ_j are given in Table A-1 for mass and momentum conservation, where σ_j is the stress tensor (containing the pressure and shear stress term), $\boldsymbol{g}$ is the gravitational acceleration,

γ is the surface tension and $\kappa \equiv \nabla \cdot \boldsymbol{n}_g$ is the surface curvature of the interface. In equations **(32)** and **(33)** it is assumed that no mass transfer occurs between the phases and that the surface tension is constant.

Table A-1 Values of Parameters for Conservation Equations

	f_j	φ_j	θ_j
Mass conservation	*1*	*0*	*0*
Momentum conservation	$\boldsymbol{u}_j$	σ_j	$\boldsymbol{g}$

The stress tensor is constructed as $\sigma_j = -p_j \mathrm{I} + \tau_j$, where p_j is the static pressure, I is the identity matrix and τ_j is the shear stress tensor. The final equations for mass and momentum for phase *j* become

$$\frac{\partial \rho_j}{\partial t} + \nabla \cdot \left(\rho_j \boldsymbol{u}_j \right) = 0, \tag{34}$$

$$\frac{\partial \rho_j \boldsymbol{u}_j}{\partial t} + \nabla \cdot \left(\rho_j \boldsymbol{u}_j \boldsymbol{u}_j \right) = -\nabla p_j + \nabla \cdot \tau_j + \rho_j \boldsymbol{g} \tag{35}$$

and the accompanying jump condition from the momentum balance across the interface

$$\left(p_g - p_l \right) \boldsymbol{n}_g + \left(\tau_l - \tau_g \right) \cdot \boldsymbol{n}_g = \gamma \kappa \boldsymbol{n}_g \tag{36}$$

where $\boldsymbol{n}_l = -\boldsymbol{n}_g$ at the interface. Consider the example of a static spherical bubble in liquid (i.e. no shear forces), equation **(36)** demonstrates that the pressure inside the bubble is higher than the hydrostatic pressure and proportional to the size (i.e. curvature) of the bubble and the surface tension.

A.1 Dimensional analysis of multiphase flow

A dimensional analysis on the fluid dynamical equations and jump conditions for a two phase system is performed. The dimension-full parameters are scaled by reference values

$$\boldsymbol{u}_j = u_{j0} \bar{\boldsymbol{u}}_j, \quad t = t_0 \bar{t}, \quad \nabla = D^{-1} \bar{\nabla}, \quad p_j = p_0 \bar{p}_j, \quad \boldsymbol{g} = g \bar{\boldsymbol{g}}, \quad \rho_j = \rho_{j0} \bar{\rho}_j, \quad \gamma = \gamma_0 \bar{\gamma}, \quad \mu_j = \mu_{j0} \bar{\mu}_j \tag{37}$$

where u_{j0} denotes the reference velocity of phase *j* (a convenient choice is the superficial velocity of phase *j* denoted by u_{sj}), *D* is the characteristic length scale (typically the diameter of the pipe) and μ_{j0} is the dynamic viscosity. The Buckingham PI theorem [4] states that the number of dimensionless parameters is equal to the number of variables minus the fundamental units (*m*, *kg* and *s*). In the case of two phase flow, equation **(35)** will yield 11 variables, so 8 dimensionless numbers will be obtained.

The momentum equation in dimensionless form can be constructed and dividing by $\rho_{j0}u_{sj}^2/D$ leads to

$$\frac{1}{\mathrm{Sl}_j}\frac{\partial\overline{\rho}_j\overline{\boldsymbol{u}}_j}{\partial\bar{t}}+\overline{\nabla}\cdot\left(\overline{\rho}_j\overline{\boldsymbol{u}}_j\overline{\boldsymbol{u}}_j\right)=-\mathrm{Eu}_j\overline{\nabla}\overline{p}_j+\frac{1}{\mathrm{Re}_j}\overline{\nabla}\cdot\bar{\tau}_j+\frac{1}{\hat{\mathrm{Fr}}_j^2}\overline{\rho}_j\overline{\boldsymbol{g}}\,. \tag{38}$$

In equation **(38)** the dimensionless groups are identified

$$\mathrm{Sl}_j\equiv\frac{D}{u_{j0}t_0}\,, \tag{39}$$

$$\mathrm{Eu}_j\equiv\frac{p_0}{\rho_{j0}u_{j0}^2}\,,$$

$$\mathrm{Re}_j\equiv\frac{\rho_{j0}u_{j0}D}{\mu_{j0}}\,,$$

$$\hat{\mathrm{Fr}}_j\equiv\frac{u_{j0}}{\sqrt{gD}}\,,$$

where Sl_j is the Strouhal number, Eu_j is the Euler number, Re_j is the Reynolds number and $\hat{\mathrm{Fr}}_j$ is the Froude number. The hat on the Froude number is to prevent confusion with the densimetric Froude number which is denoted as Fr_j.

APPENDIX B MIXTURE RULES FOR LIQUID

To obtain the dimensionless numbers for the liquid, appropriate mixing rules need to be defined. It is assumed that the liquid are well mixed and have the same velocity. The liquid density is determine by means of the well-known WLR scaling

$$\rho_l = \rho_o(1-\mathrm{WLR}) + \rho_w \mathrm{WLR}\ . \tag{40}$$

The behaviour of the liquid viscosity is very non-linear and can be described by a simplified version of the Brinkman equation [6]

$$\begin{aligned} \mu_l &= \mu_o(1-\mathrm{WLR})^{-p}, \quad \mathrm{WLR} < \mathrm{WLR}^* \\ \mu_l &= \mu_w(\mathrm{WLR})^{-p}, \qquad \mathrm{WLR} > \mathrm{WLR}^* \end{aligned} \tag{41}$$

where typically $p = 1.75$ and WLR^* is called the inversion point, which is found by matching the two expressions in equation **(41)**

$$\mathrm{WLR}^* = \frac{1}{1+\left(\frac{\mu_o}{\mu_w}\right)^{1/p}} \tag{42}$$

Determining the mixture surface tension is not evident. Every interface within the three phase mixture will have its own surface tension. In this study the surface tension is needed to determine the We_g - number for the transition between stratified and dispersed flow. It is observed that when considering the transition the oil and water phase show a volume averaged character, i.e. near the transition point a part of the oil flow becomes a dispersion while then remaining water-oil mixture is stratified. Therefore a volume flow averaging is used for the surface tension

$$\gamma_l = \gamma_o(1-\mathrm{WLR}) + \gamma_w \mathrm{WLR}\ . \tag{43}$$